Article

Investigation of Metastable Zones and Induction Times in Glycine Crystallization across Three Different Antisolvents

Lennart A. I. Ramakers,[#] John McGinty,[#] Wolfgang Beckmann, Guillaume Levilain, Mei Lee, Helen Wheatcroft, Ian Houson, and Jan Sefcik*

Cite This: https://dx.doi.org/10.1021/acs.cgd.9b01493

Read Online

ACCESS | Metrics & More | Article Recommendations

ABSTRACT: Experimental data on the effects that different antisolvents and antisolvent addition strategies have on nucleation behavior in antisolvent crystallization is very limited, and our understanding of these effects is sparse. In this work we measured the metastable zone width for the isothermal antisolvent crystallization of glycine from water utilizing methanol, ethanol, and dimethylformamide as antisolvents. We then investigated induction times for glycine crystallization across these metastable zones using the same three antisolvents. Supersaturated solutions were prepared by mixing of an antisolvent with undersaturated aqueous glycine solutions, either by batch rapid addition or using a continuous static mixer. Induction times were then recorded under agitated isothermal conditions in small vials with the use of webcam imaging and vary from apparently instant to thousands of seconds over a range of compositions and different mixing modes. Well-defined induction times were

detected across most of the metastable zone, which shows that primary nucleation is significant at supersaturations much lower than those identified in conventional metastable zone width measurements. As supersaturation increases toward the metastable zone limit, crystal growth and secondary nucleation are likely to become rate-limiting factors in the observed induction times for antisolvent crystallization. Furthermore, the observed induction times were strongly dependent on the mode of mixing (batch rapid addition vs continuous static mixing), which demonstrates an interplay of antisolvent effects on nucleation with their effects on mixing, leading to crossover of mixing and nucleation time scales. This shows that appropriate mixing strategies are crucial for the rational development of robust scalable antisolvent crystallization processes.
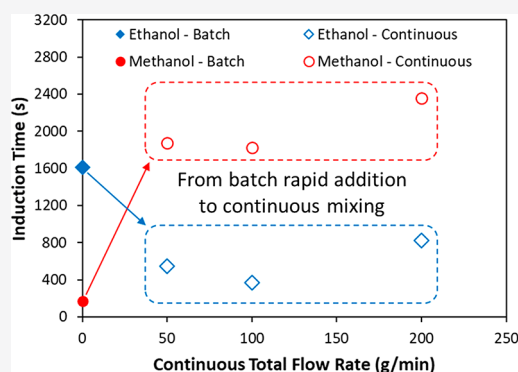
INTRODUCTION

Crystallization is often utilized as an efficient unit operation for the purification of chemicals. It is noted that, in addition to yielding a highly pure chemical product in a single step, this process also results in the production of the chemical in its solid state, which is particularly desirable within both the agrochemical and pharmaceutical industries. In solution-based crystallization, the process requires the solution to enter a supersaturated state to allow nucleation and/or growth of the solute. There are four methods of generating supersaturation: namely a reduction in temperature (cooling crystallization), the evaporation of the solvent (evaporative crystallization), a chemical reaction (reactive crystallization), and the addition of an antisolvent to the system (antisolvent crystallization). Of these four methods, the most widely studied and used is cooling crystallization due to the relative simplicity of the implementation and ease of control of this method.[1] However, not all chemicals are suitable for cooling crystallization. This can be due to the thermal instability of the chemical or a weak temperature dependence of the solubility. In these cases, it is often beneficial to utilize antisolvent crystallization, although

far less is known about antisolvent crystallization in comparison with its cooling counterpart. This is partially due to the presence of the antisolvent, making these processes three-component systems, and partially due to the need to mix the antisolvent with the solution. In order to fully understand antisolvent crystallization processes it is important to understand the interactions among the solvent, antisolvent, and solute as well as the effect of the antisolvent addition method and rate.

When the development of any crystallization process is considered, there are three key aspects which must be investigated. These can be broadly split into two separate categories, the thermodynamic and kinetic properties. The most important thermodynamic property is the solubility, and

A

the key kinetic properties are the metastable zone width (MSZW) and the induction time. For antisolvent crystallization the solubility must be determined across a range of solvent compositions, as the solvent composition is the parameter which is changed to generate supersaturation. In these systems the solubility of a solute in pure solvents or solvent mixtures is often measured by utilizing gravimetric or solid disappearance/clear point methods.[2] This has been successfully undertaken for a range of different solutes such as benzoic acid,[3,4] caffeine,[5,6] lactose,[7,8] paracetamol,[9,10] and glycine.[11−22] In these studies, it is noted that the solubility isotherms (i.e., solubility at constant temperature as a function of solvent composition) can have a range of different shapes, often involving maxima. This reflects the complex nature and range of interactions usually present in these three-component systems. Due to these complexities in antisolvent crystallization the solvent/antisolvent pair is normally chosen so that they adhere to the following requirements.

(1) The solvent/antisolvent pair should be fully miscible (with the solute dissolved) to prevent the formation of an emulsion during the crystallization process.

(2) The viscosity ratio between the solvent and antisolvent should be ≤3 to ensure that a transient emulsion does not form.[23]

(3) There should be a favorable phase diagram for antisolvent crystallization. That is, when the antisolvent is added to the solution, the solubility of the solute must decrease at a greater rate than the rate of dilution. This ensures that antisolvent addition results in a supersaturated solution.

After these initial requirements for antisolvent crystallization are satisfied, there are still many aspects of antisolvent crystallization that are not well understood. Among these is how the nature of the antisolvent and the method of mixing the antisolvent with the solution affect the crystallization outcomes.

As with cooling crystallization, the determination of the metastable zone width (MSZW) is an important aspect in the development of an antisolvent crystallization process. As such, there have been a range of studies[24−34] that have been carried out focusing on determining how to carry out such measurements and the important experimental variables. Overall, these important experimental variables have been identified as the position of the antisolvent addition port, the mixing geometry, the antisolvent addition rate, the agitation rate, the temperature, and the initial solvent composition.[27,29] It was found that the location of the addition port has an effect on the observed MSZW, which was attributed to the fact that different locations lead to the presence of a high local supersaturation for different temporal durations, leading to nucleation being triggered at different solvent compositions.[25−28] Additionally, it has been noted that increasing the agitation rate leads to a larger degree of secondary nucleation accelerating the increase in number density of nuclei within the system.[25−27] It was also found that the addition rate of the antisolvent in these systems is analogous to the cooling rate in a cooling crystallization, where an increased rate of cooling leads to a wider MSZ and shorter induction times.[25−27] Changing the temperature and initial solvent composition has been shown to modify nucleation and growth rates due to the changes in solubility and Gibbs free energy, but these effects are typically compound specific and are difficult to predict.[28,29]

Together these studies clearly demonstrate the need for further study of the kinetics of antisolvent crystallizations and the necessity to determine these important properties in a systematic way.

In this work we measured the solubilities and MSZWs in the antisolvent crystallization of glycine from water using methanol, ethanol, and N,N-dimethylformamide (DMF) as antisolvents. We then investigated induction times across the metastable zone for these antisolvents. In order to investigate the effects of mixing, induction times were measured either with batch rapid antisolvent addition or using a continuous static mixer. Particular attention was given to ensure the development of accurate and systematic methodologies to determine the kinetic properties and differences in these properties as a result of utilizing different antisolvents.

■ EXPERIMENTAL METHODS

Materials. α-Glycine (HPLC grade, purity ≥99%), ethanol (HPLC grade), methanol (reagent grade), and N,N-dimethylformamide (DMF, reagent grade) were obtained from Sigma-Aldrich and used without further purification; deionized water was obtained utilizing a Millipore Milli-Q deionized water unit (Resistivity: 15 MΩ cm). All of the experiments were carried out with the same chemical batches, ensuring that any impurities in these chemicals remained the same throughout all of the experimental work reported here.

Solubility Measurements. All solubility measurements were carried out following the procedure outlined. An excess of α-glycine (~2.5 g) was added to 5 g of solvent (pure water or water/antisolvent mixture), and this was agitated at 700 rpm in a water bath set to 25 °C for 4 days. After 4 days the stable slurries were allowed to settle for 1 h and the slurries were sampled. Approximately 2 mL of each slurry was filtered (0.2 μm Fisher syringe filter) and transferred to a preweighed 8 mL sample vial. The concentration of the saturated solution in the sample vial was then determined via gravimetric analysis (the solvent was evaporated in a vacuum oven, and the dry residue was weighed). These measurements were carried out in triplicate for a range of solvent compositions (water mass fractions 0, 0.2, 0.4, 0.6, 0.8, and 1) for each of the water/methanol, water/ethanol, and water/DMF systems. In addition to the samples taken for gravimetric analysis, a sample of the remaining suspended solid was taken and a Raman spectrum of the solid was recorded (before and after drying in a vacuum oven). The vacuum oven was operated at 25 °C at a pressure of 0.013 atm. For the water/methanol and water/ethanol systems, the solubility of α-glycine was measured as this was the polymorph present at the end of the equilibration period. For the water/DMF system, the solubility of γ-glycine was measured, as this was the polymorph present at the end of the equilibration period.

Metastable Zone Width Measurements. All MSZW measurements were carried out following the procedure outlined. Undersaturated glycine stock solutions with different water mass fractions were prepared. To ensure all of the glycine had dissolved, these solutions were stirred (at 700 rpm) and heated to 50 °C. The solutions were then held at 50 °C overnight, and after this heating period they were allowed to naturally cool to room temperature. Two gram portions of the stock solutions were transferred to 8 mL sample vials, and placed within Crystalline (Technobis) reactor chambers held at a constant temperature of 25 °C. Utilizing a syringe pump and the specially designed antisolvent addition caps (Technobis), 3.5 mL of the antisolvent was charged at an addition rate of 0.05 mL/min. The transmissivity of the sample was tracked using the inbuilt transmission meter (data collection rate: one measurement every second), and the sample was monitored using the inbuilt cameras (data collection rate: one image every 5 s). The transmission meter consisted of a laser and a detector which measured the proportion of light transmitted through the sample. The samples were agitated at 700 rpm throughout all of the MSZW measurements. For the water/ethanol system the 1, 0.8, and 0.6 water mass fraction stock solutions were prepared at 193.1, 50.2, and 10.4 g/kg solvent, respectively. For
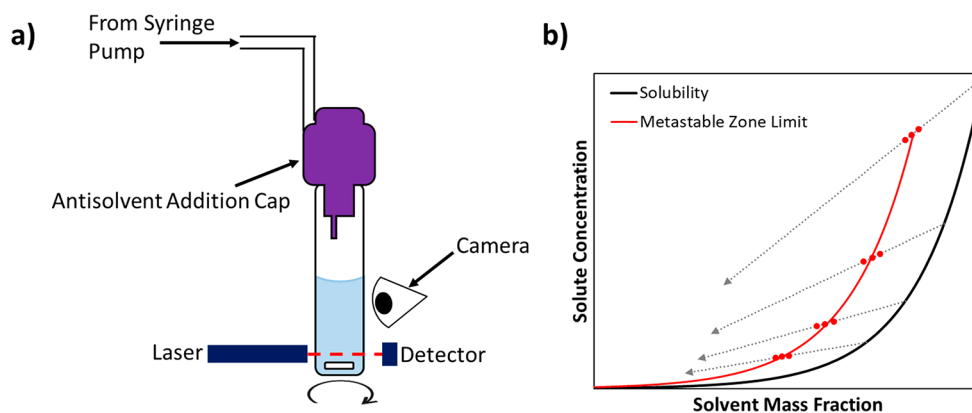
Figure 1. (a) Schematic of the Crystalline reactor (Technobis) showing the antisolvent addition cap and the inbuilt monitoring devices. (b) diagram outlining the basic methodology utilized to determine the MSZW in an isothermal antisolvent crystallization with the gray dotted lines corresponding to the dilution lines. Starting from a clear saturated solution which is sitting on the solubility curve, when antisolvent is added to this solution the trajectory across the phase diagram must follow the dilution line until nucleation occurs. This point where nucleation occurs is referred to as the metastable zone limit. There are three data points for each metastable zone limit to show the typical variability in this kind of measurement.
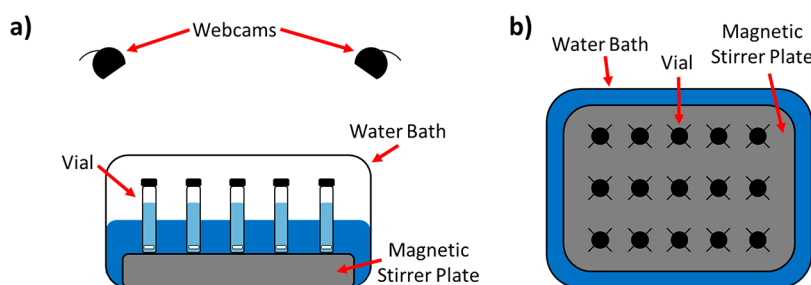
Figure 2. (a) Diagram of the side view of the custom small-scale induction platform used to measure induction times. (b) Diagram of the top view of the 15-well submersible plate in the water bath.

the water/methanol system the 1, 0.8, and 0.6 water mass fraction stock solutions were prepared at 217.7, 72.5, and 28.3 g/kg solvent, respectively. For the water/DMF system the 1, 0.95, 0.9, and 0.85 water mass fraction stock solutions were prepared at 193.1, 150.4, 78.4, and 27.5 g/kg solvent, respectively. The approach taken when these measurements were made is shown by the diagrams in Figure 1. For each measurement, the metastable limit was taken as the point when the solution became turbid (confirmed by transmission measurement and images). Three to nine repeat measurements were made under each set of conditions.

Induction Time Measurements. Glycine stock solutions with different water mass fractions were prepared. To ensure that all of the glycine had dissolved, these solutions were stirred (at 700 rpm) and heated to 50 °C. The solutions were then held at 50 °C overnight, and after this heating period they were allowed to naturally cool to room temperature. For the water/ethanol system the 1 and 0.8 water mass fraction stock solutions were prepared at concentrations of 198 and 73.6 g/kg solvent, respectively. For the water/methanol system the 1 and 0.8 solvent mass fraction stock solutions were prepared at concentrations of 198 and 72.5 g/kg solvent, respectively. For the water/DMF system the 1 water mass fraction stock solution was prepared at a concentration of 198 g/kg solvent.

Induction times were measured either by batch rapid addition or by continuous static mixing in an effort to investigate the effect of mixing on observed induction times. The batch rapid addition method involves using a pipet to inject antisolvent into a vial containing the agitated solution. This approach is similar to a full-scale batch antisolvent crystallization with the antisolvent addition being controlled by the time taken to inject the antisolvent (how quickly liquid is dispensed) and the time taken for the antisolvent to be fully distributed across the system by agitation (depends on agitation rate, agitator dimensions, and vessel size). The continuous static mixing

method involves continuously mixing the solution and antisolvent in a static mixer. Vials are then filled with this mixture and agitated. This approach could be part of a continuous antisolvent crystallization process, where the time taken for the solution and antisolvent to fully mix will be controlled by the mixer dimensions, the total flow rate, and the flow ratio. Batch addition is the conventional method used for antisolvent crystallization, but continuous mixing offers the advantages of being more controllable and scalable.

All batch rapid addition induction time measurements were carried out utilizing a custom small-scale induction platform, as shown in Figure 2. All batch rapid addition induction time measurements were carried out following the same procedure. A 2 g portion of the stock solution was transferred to each 8 mL sample vial, and the vials were placed in the water bath at 25 °C within the platform. These vials were monitored using a pair of webcams, set up to monitor the vials from the side with a data collection rate of one image every 5 s. Independent validation of the webcam sensitivity was conducted where a single vial was simultaneously monitored with a transmission probe and a webcam during an induction time experiment. The webcam always detected the onset of nucleation before the transmission probe. This suggests that the webcam is at least as sensitive as the turbidity sensors in the Crystalline reactor. Using a 1000 μL pipet (Gilson), a set volume of antisolvent was added to each vial as rapidly as possible. The exact time at which the antisolvent aliquot was added to each of the vials was recorded. The rapid addition itself was thought to take less than 2 s. Using the aqueous initial solution, for the water/ethanol system, the ethanol volumes added were 282, 362, and 447 μL. Using the aqueous initial solution, for the water/methanol system, the methanol volume added was 281 μL. Using the aqueous initial solution, for the water/DMF system, the DMF volumes added were 213, 270, 329, and 392 μL. Using the initial solution with 0.8 water mass fraction, for the water/ethanol
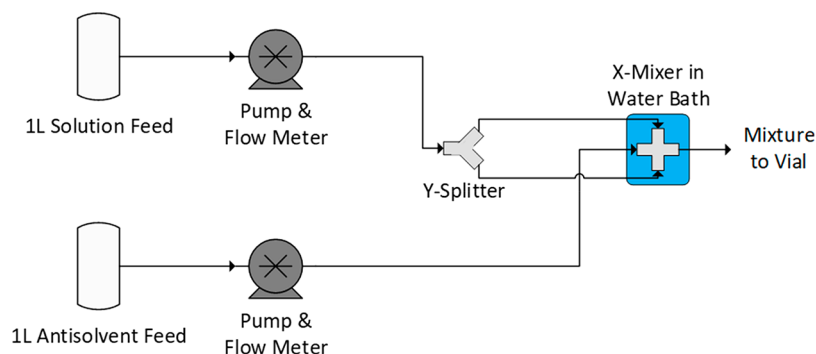
Figure 3. Diagram of the full custom continuous static mixing platform, including the X-mixer, which is used to continuously mix the solution and antisolvent.

system, the ethanol volumes added were 362 μL, 421 and 845 μL. Using the initial solution with 0.8 water mass fraction, for the water/methanol system, the methanol volumes added were 271, 566, and 842 μL. Throughout the experiments the samples were stirred at 700 rpm.

All continuous static mixing induction time experiments were carried out utilizing the custom continuous static mixing platform as shown in Figure 3. During these experiments the glycine solution is split into two separate streams using a Y-splitter and fed into the static X-mixer via opposite side input ports. The antisolvent is charged into the X-mixer via the remaining central input port. The mixture leaves from the output port of the X-mixer into 8 mL sample vials. These vials are then immediately transferred to the same small-scale induction platform used for the batch rapid addition induction time measurements (as shown in Figure 2). The vials are placed in the water bath set at 25 °C and the two webcams are used to monitor the vials from the side, allowing the induction times to be recorded. Throughout the experiment the samples were stirred at 700 rpm. The X-mixer and connected tubing all had a 1/8th in. internal diameter. The X-mixer was selected (as opposed to a T- or Y-mixer) because very uneven mass flow ratios were being used (up to 9:1) and by splitting of the larger feed the difference in flow velocities could be reduced and there would be less chance of backflow. Total flow rates of 200, 100, and 50 g/min were used during the continuous static mixing experiments, which correspond to outlet flow velocities of 0.42, 0.21, and 0.105 m/s, respectively. In the experiments using the aqueous initial glycine solution, the solution:antisolvent mass flow ratio used was 9:1. In the experiments using the initial glycine solution with water mass fraction 0.8, the solution:antisolvent mass flow ratio used was 3:1. For example, using the aqueous initial solution where the total mass flow rate was 200 g/min, the flow rates of the solution and antisolvent were 180 and 20 g/min, respectively. On the other hand, when the initial solution with water mass fraction 0.8 was used where the total mass flow rate was 200 g/min, the flow rates of the solution and antisolvent were 150 and 50 g/min, respectively. All of these flow rates were controlled with Coriolis flow meters (Bronkhorst) throughout the experiments.

Raman Spectroscopy. All Raman spectroscopy was carried out using a RamanRxn2 spectrometer (Kaiser Optical Systems, Inc.) utilizing a 785 nm laser source (class 3b) and equipped with a noncontact PhAT probe. All Raman spectra were measured over a spectral range of 150−1875 cm^{-1} at a resolution of 1 cm^{-1}, and the final spectrum presented was the average of three individual scans. The RamanRxn2 spectrometer was calibrated utilizing cyclohexane as a calibration standard, allowing the spectral range to be calibrated to an accuracy of 1 cm^{-1}. After the calibration was completed, the sample (on filter paper) was placed at the focal point of the PhAT probe within the provided black plastic sample chamber. The acquisition time of the spectrometer was then adjusted to ensure that a suitable fill factor was obtained for each sample. Each acquired spectrum was the average of three individual spectra, with the cosmic ray correction option applied within the iCRaman software. Raman spectra were recorded for the glycine crystals produced in each

experiment, both directly after filtration and after further drying in the vacuum oven. These spectra were then used to identify the polymorphic form of glycine produced in each of these experiments.

Nuclear Magnetic Resonance (NMR) Spectroscopy. For the water/DMF solubility measurements, NMR spectroscopy was used to confirm the γ-glycine solubility. In proton NMR, DMF and glycine show responses at ∼8.2 and ∼3.4 ppm, respectively. Water has a signal at ∼4.8 ppm. This means that in principle, as NMR is quantitative, the amounts of DMF and glycine can be determined using their responses, assuming they are at a low enough concentration so as not to saturate the detector in the NMR spectrometer. The filtered saturated solution samples taken from the solubility measurement experiments were diluted to a level at which the DMF was at a concentration such that it would not saturate the NMR detector. The concentrations of DMF and glycine in the diluted sample were measured using the areas of the peaks at ∼8.2 and ∼3.4 ppm, respectively. The concentration of glycine in the original sample, prior to the dilution, was then calculated.

■ RESULTS AND DISCUSSION

Solubility Measurements. The literature reports a large number of glycine solubility measurements in water.[11−17,20,22,35−37] However, the literature exhibits a large degree of variability for aqueous glycine solubility. For temperatures between 20 and 25 °C, the solubility ranges from ∼140 to ∼250 g/kg water. Beyond this initial observation the literature also shows that the solubility of γ-glycine is lower than the solubility of α-glycine at both 20 and 25 °C, which is consistent with the fact that γ-glycine is thermodynamically the most stable polymorphic form.[36] Additionally, solubility values of β-glycine appear to be greater than those for the other polymorphs, which is consistent with the reported metastable nature of this form.[37] It should be noted that in ∼73% of the studies collated here the polymorph of the glycine used to measure the aqueous solubility is not specified. Due to the large degree of variation in the aqueous solubility values found in the literature, the solubility of α-glycine in water was measured using the method outlined in this work. From these measurements the aqueous solubility was found to be 245 g/kg solvent at 25 °C, which is consistent with the most common values seen in the literature.

As glycine is an amino acid, its aqueous solubility depends on pH and this could potentially be another source of variation in the glycine solubility measurements. It can be seen from the literature that a pure aqueous glycine solution will have a pH value of ∼6 and that there is almost no change in the aqueous solubility of glycine between pH 4 and pH 8.[18,35,36] For these reasons it was concluded that the pH would not change so significantly in our measurements that it could affect the
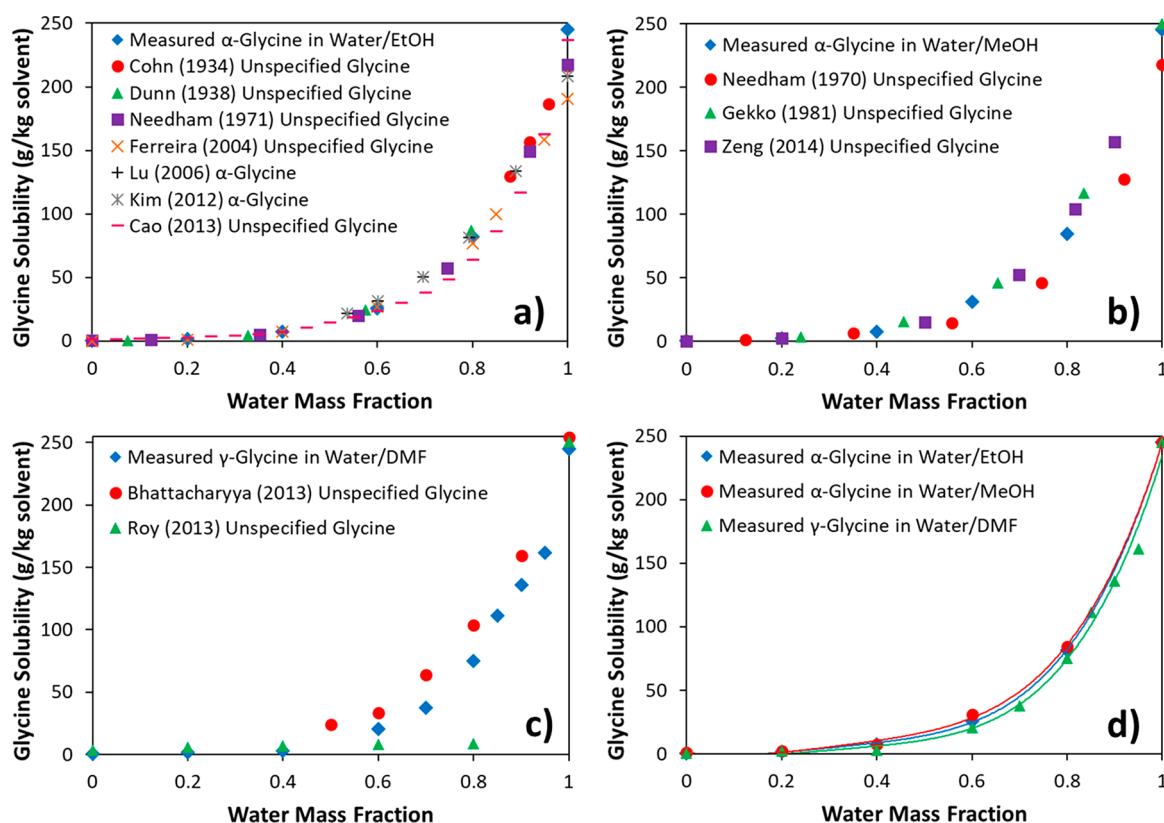
Figure 4. Comparison of experimentally measured and literature data for the glycine solubility curves in (a) water/ethanol,[11−16,18] (b) water/methanol,[18−20] and (c) water/DMF[21,22] solvent mixtures, in addition to (d) a comparison of experimentally measured solubility curves. In (d), most of the water/ethanol data points are obscured by the water/methanol data points due to their similarity. The measured solubility values were taken at 25 °C. The literature solubility values were taken between 20 and 25 °C.

solubility value and so the pH value was not measured in this work.

In addition to the large number of solubility values determined for glycine in water, a range of studies have been carried out on the solubility of glycine in binary aqueous/organic solvent mixtures.[12−15,18−22,37] In these aqueous/organic solvent mixtures the organic component is often chosen such that glycine is poorly soluble in the pure organic component. In this work the solubility curves of α-glycine in the water/ethanol and water/methanol systems were determined at 25 °C. In addition, the solubility curve of γ-glycine in the water/DMF system was also determined at 25 °C. These solubility curves are shown and compared with the literature solubility curves in Figure 4a−c. As seen for the literature aqueous glycine solubility values, there is a spread in the solubility curves observed for glycine in the water/ethanol, water/methanol, and water/DMF systems.

In this work, at the end of the solubility measurements for these systems the remaining undissolved solid was isolated and solid-state analysis was performed using Raman spectroscopy. For both the water/ethanol and water/methanol systems it was noted that the remaining solid in all of the samples was α-glycine and so it can be stated that the α-glycine solubility curves were measured for these two systems. For the water/DMF system the remaining solid in all of the samples was γ-glycine and so it can be stated that the γ-glycine solubility curve was measured for this system.

In contrast to the water/ethanol and water/methanol systems it is noted that there are only two studies where the solubility of glycine in the water/DMF system has been

explored (Figure 4c). Furthermore, the two literature solubility curves for the DMF/water system are substantially different. One of these curves was determined via gravimetric analysis,[21] while the other curve was obtained utilizing a formol titration.[22] It is noted that the solubility values obtained implementing gravimetric analysis are much higher than those obtained by the formol titration. It is thought that this large discrepancy between the solubility curves for the water/DMF system obtained by these two different methods could be caused by a number of different factors. On the one hand, it is thought that the gravimetric analysis of the solubility of glycine in the water/DMF system could overestimate the values due to the low volatility of DMF (it is very difficult to remove DMF from the sample). On the other hand, it is possible that the solubility values obtained via formol titration are underestimated due to the neutralization of the formaldehyde which takes place during the titration process (it is easy to overshoot formaldehyde neutralization and produce excess base). Additionally, the polymorph of glycine used in these studies is not specified, meaning that it is possible that part of the discrepancy between these values is due to the difference in the solubility of α- and γ-glycine. In this study, the solubility of glycine in the water/DMF system was determined using both gravimetric analysis and NMR spectroscopy, utilizing the DMF present in the original solvent mixture as an internal standard. It is the values from the gravimetric analysis which are shown in Figure 4c,d. Overall, the experimentally measured solubility curves (Figure 4d) obtained here for the three different solvent systems are similar. It is noted that the water/DMF solubility curve shows that the solubility in this system is slightly lower

than in the water/ethanol and water/methanol systems; however, this is thought to be consistent with the fact that it is γ-glycine which is present. It is known that the solubility ratio of α-glycine to γ-glycine is 1.12.[36]

MSZW Measurements. The MSZWs for glycine in the three water/antisolvent systems were compared to assess the effect of changing the antisolvent on the MSZW. This comparison is shown in Figure 5.
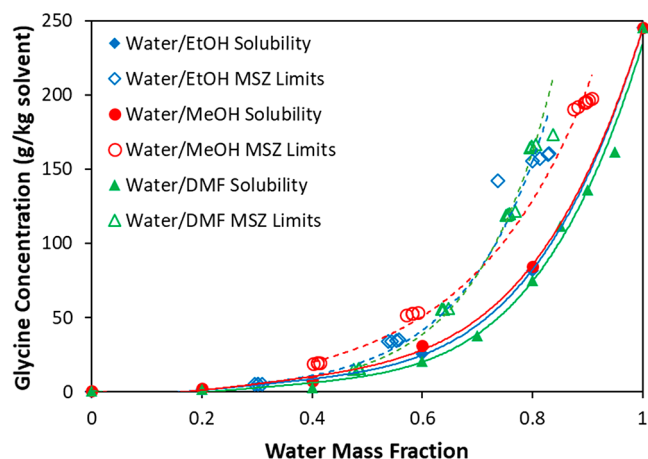

Figure 5. Comparison among the MSZWs for glycine in the water/ethanol, water/methanol, and water/DMF systems.

On comparison of the MSZWs for these three different systems it can be seen that the MSZWs for the water/ethanol and water/DMF systems are very similar. In contrast to this, the MSZW of the water/methanol system is narrower when the initial glycine solution is purely aqueous but wider when the initial glycine solution has a greater antisolvent mass fraction. Overall, the MSZWs for all three antisolvents are broadly similar despite the differences in the precise shapes. It was determined that it was not possible to compare the MSZWs from the antisolvent crystallization of glycine with the MSZWs from the cooling crystallization of aqueous glycine due to the inherently different physical processes taking place.

Raman spectroscopy was used to determine the glycine polymorph obtained in these MSZW experiments. For all of these systems it is noted that when the composition of the initial solution is above 0.75 water mass fraction the addition of antisolvent yields α-glycine. However, it was found for the water/ethanol and water/methanol systems that when the initial solution contained the water mass fraction 0.6 the addition of antisolvent led to the production of β-glycine. From Raman spectra, it appeared to be pure β-glycine but due to the instrument's limit of detection there could have been a small amount of other polymorphs present. It is thought that β-glycine is obtained due to the high amount of antisolvent initially present in these solutions, which is consistent with a literature report that the transformation from β-glycine to α-glycine takes longer with increasing antisolvent fraction.[37] While β-glycine was obtained over a wide range of methanol and ethanol concentrations in previous studies under unstirred conditions,[38] stirring was found to strongly favor α-glycine in aqueous solutions[39,40] and a similar effect may play a role in mixed solvents.

Induction Time Measurements. The results of induction time measurements using the batch rapid addition experiments are presented in Figure 6. MSZ limits are also included in Figure 6 and are taken from the MSZW experiments where the corresponding initial solution compositions and antisolvents were used. This comparison between induction times and MSZ limits is being made on the basis of supersaturation. In this work, supersaturation (S) is defined as the ratio of solution concentration to saturation concentration. For the three antisolvents used, there was little difference between induction times at similar supersaturations ($1.34 \leq S \leq 1.72$). At lower supersaturations ($S \leq 1.33$) induction times are very long, as expected. However, at higher supersaturations the induction times are relatively short, are similar among different antisolvents, and are only weakly dependent on supersaturation. Furthermore, primary nucleation within the MSZs is not only dependent on the antisolvent selected but also on the initial compositions of the solution. To interpret these results correctly, it should be remembered that Mullin[41] defined the observed induction time as the summation of the relaxation time (time required for the system to reach a quasi steady state), the nucleation time (time required for a nucleus to form), and the growth time (time required for the nucleus to grow to a detectable size and/or the time for secondary
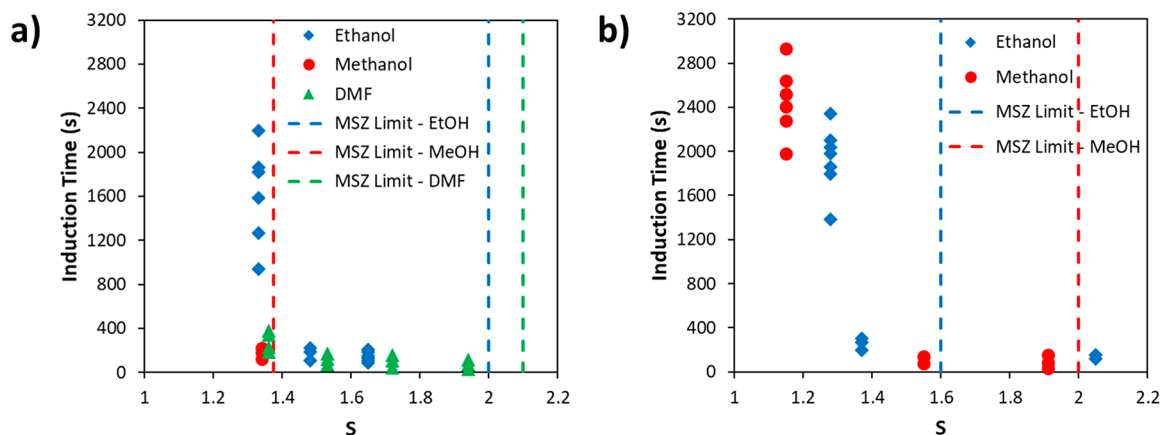
Figure 6. (a) Measured induction times (closed symbols) and MSZ limits (vertical dashed lines) as a function of supersaturation in the water/ethanol (blue diamonds), water/methanol (red circles) and water/DMF (green triangles) systems at 25 °C from aqueous initial solutions. (b) Measured induction times (closed symbols) and MSZ limits (vertical dashed lines) as a function of supersaturation in the water/ethanol (blue diamonds) and water/methanol (red circles) systems at 25 °C from initial solutions with a water mass fraction of 0.8.
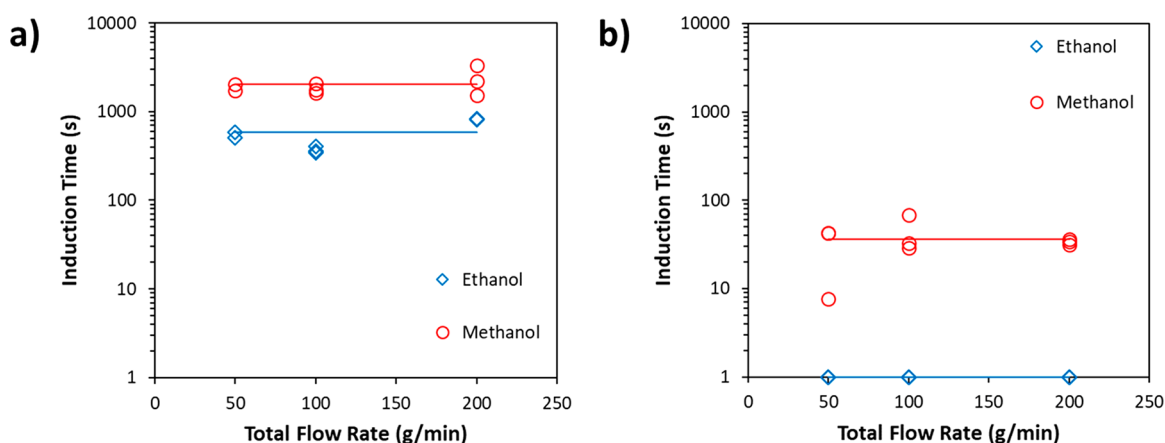
Figure 7. Induction times from continuous static mixing experiments using (a) an aqueous initial solution or (b) an initial solution with 0.8 water mass fraction. All experiments were performed at 25 °C. Three induction times are shown for each flow rate used. The mean induction times for each set of conditions are shown as horizontal lines.

nucleation to increase the number of nuclei to the point where they are detectable).

The fact that at higher supersaturations the induction times become much less dependent on supersaturation suggests that the relaxation time and nucleation time are likely to become negligible, whereas crystal growth (limited by mass transport or surface integration) and secondary nucleation (limited by mechanical action), both of which only weakly (up to linearly) depend on supersaturation, become important factors. Furthermore, in the context of antisolvent crystallization, it is known that the glycine crystal growth rate decreases with increasing antisolvent content at a given supersaturation.[38,42] These factors indicate that, as supersaturation increases, crystal growth and secondary nucleation may become rate-limiting factors in observed induction times in antisolvent crystallization.

Unlike the MSZW data, it is possible to directly compare induction times from the antisolvent crystallization of glycine in this work with induction times from the cooling crystallization of aqueous glycine presented in the literature to gain a better understanding of the effect of the antisolvents. One study[43] was found which observed agitated solutions at similar supersaturations and temperatures, and it can be seen that for antisolvent crystallization, at a supersaturation of around 1.15, the induction time is on average 5 times longer than that for its cooling counterpart. This can possibly be explained by the findings of a different study,[42] which demonstrated that the growth rate of glycine is 5−10 times slower in water/methanol solvent mixtures than in purely aqueous solutions. The difference in growth rate is important because, using Mullin's definition of observed induction time, the antisolvent and cooling crystallizations of glycine may have very similar relaxation and nucleation times but significantly different growth times, which leads to significantly different observed induction times. This demonstrates that differences in observed induction time cannot simply be explained by differences in primary nucleation across wide range of supersaturations, especially with variable solvent mixture compositions.

The effect of mixing on the induction time was also explored for the water/ethanol and water/methanol systems by utilizing the continuous static mixing platform. The results of these continuous static mixing experiments are presented in Figure 7.

Table 1 shows the mean induction times from the continuous static mixing experiments alongside the batch

Table 1. Comparison between the Mean Induction Times from the Continuous Static Mixing Experiments and the Comparable Batch Rapid Addition Experiments

mixing method	initial water mass fraction	antisolvent	supersaturation	mean induction time (s)
batch rapid addition	1	ethanol	1.33	1610
batch rapid addition	1	methanol	1.34	168
batch rapid addition	0.8	ethanol	2.05	135
batch rapid addition	0.8	methanol	1.91	70
continuous mixing	1	ethanol	1.33	584
continuous mixing	1	methanol	1.34	2036
continuous mixing	0.8	ethanol	2.05	1
continuous mixing	0.8	methanol	1.91	36

rapid addition experiments with which they are being compared. The experimental conditions used in these experiments are also shown.

The induction times observed when aqueous initial solutions were used were longer than those when initial solutions of 0.8 water mass fraction was used, and this can be attributed to the lower relative supersaturations achieved on starting from aqueous initial solutions. For aqueous initial solutions, an investigation of the mixing effects showed that using continuous mixing with the ethanol antisolvent decreased the induction times by up to 1 order of magnitude in comparison to batch rapid antisolvent addition. Surprisingly, an opposite effect was seen with the methanol antisolvent, where using continuous mixing increased the induction times by up to 2 orders of magnitude in comparison to batch rapid antisolvent addition. For initial solutions with 0.8 water mass fraction, we can see that using continuous mixing with the ethanol antisolvent decreased the induction times by at least 2 orders of magnitude from over 2 min to less than 1 s (crystals were

G

observed in the mixture leaving the continuous mixing platform with a residence time of <1 s), while using continuous mixing with the methanol antisolvent did not have a significant effect on the induction times. For both initial solutions, the induction times with the ethanol antisolvent were higher than those with the methanol antisolvent for batch rapid antisolvent addition. However, the opposite was found for continuous mixing. This raises intriguing questions about how the effects of solvent and mixing conspire to switch relative magnitudes of induction times between methanol and ethanol antisolvents.

First, let us consider the effects of antisolvents on induction times separately from those of mixing. Different antisolvents can lead to different solubility and different activity coefficients in nonideal mixtures (which can result in differences in the driving force for nucleation), different nucleation barrier heights (due to different surface energies) and kinetic prefactors (which can result in differences in nucleation rate constants), and different crystal growth rates and secondary nucleation rates (which can result in different time scales contributing to detected induction times[44]). The effects of differences in solubility and solution nonideality can be addressed by adjusting the driving forces: for example, working at the same supersaturations (while accounting for relative changes in ratios of solute activity coefficients if not negligible), as we have done here. The effects of crystal growth rates and secondary nucleation rates can be addressed separately[45] and accounted for as appropriate. Once these are accounted for, the effects of antisolvents on nucleation kinetics as such as can be assessed properly, assuming no other effects are involved. However, as we have seen above, mixing effects can also play a crucial role.

Second, let us consider the effects of mixing on induction times separately from those of antisolvents. Ideally, we would want a mixing process to provide a homogeneous solution where the initial solution and the antisolvent are fully mixed to achieve the resulting mixture concentration at time scales shorter than those of subsequent events leading to nucleation and growth of crystals. While this may be possible under certain circumstances, often there are local concentration heterogeneities introduced during the mixing process where nucleation rates become sufficiently high at certain locations to yield crystal nuclei under conditions different from those corresponding to the resulting mixture concentration. Time scales of mixing depend on the energy input provided for mixing (through impeller power or pressure drop in static mixers) which is acting locally through a spatially distributed energy dissipation rate[46] under turbulent mixing conditions, while microscale homogeneity is ultimately achieved through diffusive mixing. Different antisolvents can have different densities and viscosities (which can result in different distributions of energy dissipation rates across mixing volumes) and also different mutual diffusion coefficients with solution components, which can result in different transient concentration profiles along temporary interfaces between the antisolvent and the initial solution while diffusive mixing is acting to achieve microscale homogeneity in the resulting mixture. This can lead to significant transient increases in local supersaturation well above the final value corresponding to the resulting mixture concentration.[47] In the case of ethanol and methanol as antisolvents, while the densities of ethanol and methanol are similar, the viscosity of ethanol and aqueous ethanol mixtures is about twice that of methanol and aqueous methanol mixtures, respectively, while the mutual diffusion

coefficients of ethanol and water are 2−3 times lower than those of methanol and water in alcohol-rich aqueous solutions.[48,49] Therefore, changing mixing conditions will have different effects for different antisolvents and will result in different mixing time scales as well as different magnitudes and durations of local concentration heterogeneities facilitating spatially and temporarily located nucleation.

When we now consider the effects of antisolvents on induction times under well-mixed conditions together with the effects of antisolvents on the mixing process, we can see that there is an interplay which can lead to a crossover of mixing and nucleation time scales. Various factors discussed above may play roles in decreasing or increasing observed induction times, depending on which factors become rate determining under each set of mixing conditions. While it has not been our aim here to deconvolute these factors for the particular systems investigated here, it is clear that careful analysis of antisolvent effects on nucleation and growth kinetics under well-mixed conditions studied separately from antisolvent effects in mixing and local concentration heterogeneities is needed in order to properly understand and interpret antisolvent effects on induction times and primary nucleation kinetics in antisolvent crystallization.

■ CONCLUSIONS

The isothermal metastable zone widths for glycine antisolvent crystallization using three different antisolvents were found to be similar. Well-defined induction times were observed across the metastable zones which show that primary nucleation is significant at supersaturations much lower than those identified in conventional metastable zone width measurements. As supersaturation increases toward the metastable zone limit, other factors are likely to become rate limiting, including crystal growth and secondary nucleation, as well as mixing, which need to be considered when induction time data are interpreted in terms of primary nucleation kinetics, as is commonly done in the literature. Surprisingly, we found that induction times for the ethanol antisolvent were higher than those for the methanol antisolvent under batch rapid addition, while the opposite was the case under continuous mixing. This shows that there is an interplay of antisolvent effects on nucleation and growth with effects on mixing, which can lead to a crossover of mixing and nucleation time scales. Overall, induction times are strongly dependent on the mode of mixing (batch rapid addition vs continuous mixing) which shows that appropriate mixing strategies are crucial for the rational development of robust, scalable antisolvent crystallization processes.

■ AUTHOR INFORMATION

Corresponding Author

Jan Sefcik − *Future Manufacturing Research Hub in Continuous Manufacturing and Advanced Crystallisation, Department of Chemical and Process Engineering, University of Strathclyde, Glasgow G1 1XJ, U.K.*; Email: jan.sefcik@strath.ac.uk

Authors

Lennart A. I. Ramakers − *Future Manufacturing Research Hub in Continuous Manufacturing and Advanced Crystallisation, Department of Chemical and Process Engineering, University of Strathclyde, Glasgow G1 1XJ, U.K.*

John McGinty − *Future Manufacturing Research Hub in Continuous Manufacturing and Advanced Crystallisation,*

Department of Chemical and Process Engineering, University of Strathclyde, Glasgow G1 1XJ, U.K.; ● orcid.org/0000-0002-8166-7266

Wolfgang Beckmann − *Bayer AG, Research & Development, Pharmaceuticals, Material Science, 42096 Wuppertal, Germany*

Guillaume Levilain − *Bayer AG, Research & Development, Pharmaceuticals, Material Science, 42096 Wuppertal, Germany*

Mei Lee − *Product Development and Supply, GlaxoSmithKline, Stevenage, Hertfordshire SG1 2NY, U.K.*

Helen Wheatcroft − *Chemical Development, Pharmaceutical Technology & Development, AstraZeneca, Macclesfield SK10 2NA, U.K.*

Ian Houson − *Future Manufacturing Research Hub in Continuous Manufacturing and Advanced Crystallisation, University of Strathclyde, Glasgow G1 1XJ, U.K.*

Complete contact information is available at:
https://pubs.acs.org/10.1021/acs.cgd.9b01493

Author Contributions

[#]L.A.I.R. and J.M. contributed equally to this work.

Notes

The authors declare no competing financial interest.

■ REFERENCES

(1) Brown, C. J.; McGlone, T.; Yerdelen, S.; Srirambhatla, V.; Mabbott, F.; Gurung, R.; Briuglia, M. L.; Ahmed, B.; Polyzois, H.; McGinty, J.; Perciballi, F.; Fysikopoulos, D.; MacFhionnghaile, P.; Siddique, H.; Raval, V.; Harrington, T. S.; Vassileiou, A. D.; Robertson, M.; Prasad, E.; Johnston, A.; Johnston, B.; Nordon, A.; Srai, J. S.; Halbert, G.; ter Horst, J. H.; Price, C. J.; Rielly, C. D.; Sefcik, J.; Florence, A. J. Enabling precision manufacturing of active pharmaceutical ingredients: workflow for seeded cooling continuous crystallisations. *Mol. Syst. Des. Eng.* **2018**, *3*, 518−549.

(2) Hossain, A.; Roy, S.; Dolui, B. K. Effects of thermodynamics on the solvation of amino acids in the pure and binary mixtures of solutions: A review. *J. Mol. Liq.* **2017**, *232*, 332−350.

(3) Chertkoff, M. J.; Martin, A. N. The solubility of Benzoic Acid in mixed solvents. *J. Am. Pharm. Assoc., Sci. Ed.* **1960**, *49*, 444−447.

(4) Thati, J.; Nordstrom, F. L.; Rasmuson, A. C. Solubility of Benzoic Acid in Pure Solvents and Binary Mixtures. *J. Chem. Eng. Data* **2010**, *55*, 5124−5127.

(5) Herrador, M. A.; Gonzalez, A. G. Solubility prediction of caffeine in aqueous N, N-dimethylformamide mixtures using the Extended Hildebrand Solubility Approach. *Int. J. Pharm.* **1997**, *156*, 239−244.

(6) Adjei, A.; Newburger, J.; Martin, A. Extended Hildebrand approach - Solubility of Caffeine in Dioxane-Water mixtures. *J. Pharm. Sci.* **1980**, *69*, 659−661.

(7) Brito, A. B. N.; Giulietti, M. Study of lactose crystallization in water-acetone solutions. *Cryst. Res. Technol.* **2007**, *42*, 583−588.

(8) Machado, J. J. B.; Coutinho, J. A. P.; Macedo, E. A. Solid-liquid equilibrium of alpha-lactose in ethanol/water. *Fluid Phase Equilib.* **2000**, *173*, 121−134.

(9) Romero, S.; Reillo, A.; Escalera, B.; Bustamante, P. The behavior of paracetamol in mixtures of amphiprotic and amphiprotic-aprotic solvents. Relationship of solubility curves to specific and nonspecific interactions. *Chem. Pharm. Bull.* **1996**, *44*, 1061−1064.

(10) Granberg, R. A.; Ducreux, C.; Gracin, S.; Rasmuson, A. C. Primary nucleation of paracetamol in acetone-water mixtures. *Chem. Eng. Sci.* **2001**, *56*, 2305−2313.

(11) Dunn, M. S.; Ross, F. J.; Read, L. S. The solubility of the amino acids in water*. *J. Biol. Chem.* **1933**, *103*, 579−595.

(12) Kim, J. W.; Koo, K. K. Crystallization of Glycine by Drowning-Out Combined with Fines Dissolution and Cooling Process with in Situ Control using Focused Beam Reflectance Measurement and Attenuated Total Reflection-Fourier Transform Infrared Spectroscopy. *Cryst. Growth Des.* **2012**, *12*, 4927−4934.

(13) Cao, Z.; Hu, Y. H.; Li, J. J.; Kai, Y. M.; Yang, W. G. Solubility of glycine in binary system of ethanol plus water solvent mixtures: Experimental data and thermodynamic modeling. *Fluid Phase Equilib.* **2013**, *360*, 156−160.

(14) Ferreira, L. A.; Macedo, E. A.; Pinho, S. P. Solubility of amino acids and diglycine in aqueous-alkanol solutions. *Chem. Eng. Sci.* **2004**, *59*, 3117−3124.

(15) Cohn, E. J.; McMeekin, T. L.; Edsall, J. T.; Weare, J. H. Studies in the physical chemistry of amino acids, peptides and related substances. II the solubility of a-ammo acids in water and in alcohol-water mixtures. *J. Am. Chem. Soc.* **1934**, *56*, 2270−2282.

(16) Lu, J.; Wang, X. J.; Yang, X.; Ching, C. B. Solubilities of glycine and its oligopeptides in aqueous solutions. *J. Chem. Eng. Data* **2006**, *51*, 1593−1596.

(17) Needham, T. E.; Paruta, A. N.; Gerraughty, R. J. Solubility of amino acids in pure solvent systems. *J. Pharm. Sci.* **1971**, *60*, 565−567.

(18) Needham, T. E.; Paruta, A. N.; Gerraughty, R. J. Solubility of amino acids in mixed solvent systems. *J. Pharm. Sci.* **1971**, *60*, 258−260.

(19) Zeng, Y.; Li, Z. B.; Demopoulos, G. P. Phase Equilibria for the Glycine-Methanol-NH4Cl-H2O System. *Ind. Eng. Chem. Res.* **2014**, *53*, 16864−16872.

(20) Gekko, K. Mechanism of polyol-induced protein stabilization - Solubility of amino-acids and diglycine in aqueous polyol solutions. *J. Biochem.* **1981**, *90*, 1633−1641.

(21) Bhattacharyya, A.; Bhattacharya, S. K. Chemical Transfer Energies of Some Homologous Amino Acids and the -CH2- Group in Aqueous DMF: Solvent Effect on Hydrophobic Hydration and Three Dimensional Solvent Structure. *J. Solution Chem.* **2013**, *42*, 2149−2167.

(22) Roy, S.; Mahali, K.; Dolui, B. K. Thermodynamic Interactions Due to Transfer of Amino Acids, Glycine and DL-Alanine from Water to Aqueous Mixture of Cationophilic Dipolar Aprotic N, N-Dimethyl Formamide. *Asian J. Chem.* **2013**, *25*, 8037−8042.

(23) Wang, X.; Gillian, J. M.; Kirwan, D. J. Quasi-emulsion precipitation of pharmaceuticals. 1. Conditions for formation and crystal nucleation and growth behavior. *Cryst. Growth Des.* **2006**, *6*, 2214−2227.

(24) Trifkovic, M.; Sheikhzadeh, M.; Rohani, S. Determination of metastable zone width for combined anti-solvent/cooling crystallization. *J. Cryst. Growth* **2009**, *311*, 3640−3650.

(25) O'Grady, D.; Barrett, M.; Casey, E.; Glennon, B. The effect of mixing on the metastable zone width and nucleation kinetics in the anti-solvent crystallization of benzoic acid. *Chem. Eng. Res. Des.* **2007**, *85*, 945−952.

(26) Chaitanya, K. K.; Sarkar, D. Determination of the Metastable Zone Width by a Simple Optical Probe. *Chem. Eng. Technol.* **2014**, *37*, 1037−1042.

(27) Kubota, N. An interpretation of the metastable zone width concerning primary nucleation in anti-solvent crystallization. *J. Cryst. Growth* **2008**, *310*, 4647−4651.

(28) Zhang, Y.; Jiang, Y. B.; Zhang, D. K.; Qian, Y.; Wang, X. Z. Metastable zone width, crystal nucleation and growth kinetics measurement in anti-solvent crystallization of beta-artemether in the mixture of ethanol and water. *Chem. Eng. Res. Des.* **2015**, *95*, 187−194.

(29) El Bazi, W.; Abou Jaoude, M. T. M.; Porte, C.; Mabille, I.; Havet, J. L. Isothermal crystallization of glycine in semi-continuous mode by anti-solvent addition. *J. Cryst. Growth* **2018**, *498*, 202−208.

(30) Simone, E.; Tyler, A. I. I.; Kuah, D.; Bao, X. F.; Ries, M. E.; Baker, D. Optimal Design of Crystallization Processes for the Recovery of a Slow-Nucleating Sugar with a Complex Chemical Equilibrium in Aqueous Solution: The Case of Lactose. *Org. Process Res. Dev.* **2019**, *23*, 220−233.

(31) Kaskiewicz, P. L.; Xu, G. Y.; Lai, X. J.; Warren, N. J.; Roberts, K. J.; Morton, C.; Dowding, P.; George, N. Isothermal by Design: An Accelerated Approach to the Prediction of the Crystallizability of Slowly Nucleating Systems. *Org. Process Res. Dev.* **2019**, *23*, 1948−1959.

I

(32) Raza, S. A.; Schacht, U.; Svoboda, V.; Edwards, D. P.; Florence, A. J.; Pulham, C. R.; Sefcik, J.; Oswald, L. D. H. Rapid Continuous Antisolvent Crystallization of Multicomponent Systems. *Cryst. Growth Des.* **2018**, *18*, 210−218.

(33) MacFhionnghaile, P.; Svoboda, V.; McGinty, J.; Nordon, A.; Sefcik, J. Crystallization Diagram for Antisolvent Crystallization of Lactose: Using Design of Experiments To Investigate Continuous Mixing-Induced Supersaturation. *Cryst. Growth Des.* **2017**, *17*, 2611− 2621.

(34) Svoboda, V.; MacFhionnghaile, P.; McGinty, J.; Connor, L. E.; Oswald, I. D. H.; Sefcik, J. Continuous Cocrystallization of Benzoic Acid and Isonicotinamide by Mixing-Induced Supersaturation: Exploring Opportunities between Reactive and Antisolvent Crystal-lization Concepts. *Cryst. Growth Des.* **2017**, *17*, 1902−1909.

(35) Fuchs, D.; Fischer, J.; Tumakaka, F.; Sadowski, G. Solubility of amino acids: Influence of the pH value and the addition of alcoholic cosolvents on aqueous solubility. *Ind. Eng. Chem. Res.* **2006**, *45*, 6578−6584.

(36) Yang, X.; Wang, X.; Ching, C. B. Solubility of form alpha and form gamma of glycine in aqueous solutions. *J. Chem. Eng. Data* **2008**, *53*, 1133−1137.

(37) Bouchard, A.; Hofland, G. W.; Witkamp, G. J. Solubility of glycine polymorphs and recrystallization of beta-glycine. *J. Chem. Eng. Data* **2007**, *52*, 1626−1629.

(38) Weissbuch, I.; Torbeev, V. Y.; Leiserowitz, L.; Lahav, M. Solvent effect on crystal polymorphism: Why addition of methanol or ethanol to aqueous solutions induces the precipitation of the least stable beta form of glycine. *Angew. Chem., Int. Ed.* **2005**, *44*, 3226− 3229.

(39) Renuka Devi, K.; Gnanakamatchi, V.; Srinivasan, K. Attainment of unstable beta nucleation of glycine through novel swift cooling crystallization process. *J. Cryst. Growth* **2014**, *400*, 34−42.

(40) Vesga, M. J.; McKechnie, D.; Mulheran, P. A.; Johnston, K.; Sefcik, J. Conundrum of gamma glycine nucleation revisited: to stir or not to stir? *CrystEngComm* **2019**, *21*, 2234−2243.

(41) Mullin, J. *Crystallization*, 4th ed.; Butterworth-Heinemann: Oxford, U.K., 2001.

(42) El Bazi, W.; Porte, C.; Mabille, I.; Havet, J. L. Antisolvent crystallization: Effect of ethanol on batch crystallization of alpha glycine. *J. Cryst. Growth* **2017**, *475*, 232−238.

(43) Shiau, L. D. Determination of the Nucleation and Growth Kinetics for Aqueous L-glycine Solutions from the Turbidity Induction Time Data. *Crystals* **2018**, *8*, 403.

(44) Sohnel, O.; Mullin, J. W. Interpretation of Crystallization Induction Periods. *J. Colloid Interface Sci.* **1988**, *123*, 43−50.

(45) Briuglia, M. L.; Sefcik, J.; ter Horst, J. H. Measuring Secondary Nucleation through Single Crystal Seeding. *Cryst. Growth Des.* **2019**, *19*, 421−429.

(46) Marchisio, D. L.; Soos, M.; Sefcik, J.; Morbidelli, M.; Barresi, A. A.; Baldi, G. Effect of fluid dynamics on particle size distribution in particulate processes. *Chem. Eng. Technol.* **2006**, *29*, 191−199.

(47) Bhamidi, V.; Lee, S. H.; He, G. W.; Chow, P. S.; Tan, R. B. H.; Zukoski, C. F.; Kenis, P. J. A. Antisolvent Crystallization and Polymorph Screening of Glycine in Microfluidic Channels Using Hydrodynamic Focusing. *Cryst. Growth Des.* **2015**, *15*, 3299−3306.

(48) Derlacki, Z. J.; Easteal, A. J.; Edge, A. V. J.; Woolf, L. A.; Roksandic, Z. Diffusion-coefficients of Methanol and Water and the mutual diffusion-coefficient in Methanol-Water solutions at 278-K and 298-K. *J. Phys. Chem.* **1985**, *89*, 5318−5322.

(49) Pratt, K. C.; Wakeham, W. A. Mutual diffusion-coefficient of Ethanol-Water mixtures - Determination by a rapid, new method. *Proc. R. Soc. London, Ser. A* **1974**, *336*, 393−406.